Sigma Journal of Engineering and Natural Sciences
Web page info: https://sigma.yildiz.edu.tr
DOI: 10.14744/sigma.2026.1963

Research Article

Effect of coconut shell biochar on the flexural properties of polylactic acid bio-composite filaments for fused deposition modeling

Vishal DHIMMAR[1,2,*], Saurin SHETH[3]

[1]*Charutar Vidya Mandal University, Gujarat, 388120, India*
[2]*S. N. Patel Institute of Technology, Gujarat Technological University, Gujarat, 394601, India*
[3]*G. H. Patel College of Engineering and Technology, Charutar Vidya Mandal University, Gujarat, 388120, India*

ARTICLE INFO

Article history
Received: 20 January 2025
Revised: 31 May 2025
Accepted: 01 July 2025

Keywords:
Additive Manufacturing; Bio-Composite Filament; FDM

ABSTRACT

Synthetic fibers can improve mechanical performance, as they stiffen polymer parts, but they come from non-renewable sources. So that has pushed researchers toward natural fillers. We blended coconut shell biochar (CBC), pyrolyzed at 400 °C, into PLA filament and printed flexural specimens by FDM to see what the filler does to bending performance. Three factors were varied: CBC content (0, 3, 6, and 9 wt%), infill pattern, and layer thickness. A small amount helped. At 3 wt%, mean flexural strength rose from 93.3 to 113.4 MPa and modulus from 3056 to 3367 MPa, but both fell below the unfilled values at 6 and 9 wt%, while strain kept climbing. Infill pattern mattered too: parallel (0°) printing gave the strongest and stiffest parts, up to 124.8 MPa at 3 wt% CBC and 0.25 mm. When all three responses were optimized together, however, the best setting was unfilled PLA with parallel infill and 0.15 mm layers, and confirmation prints came within about 1.5% of the predictions.

Cite this article as: Dhimmar V, Sheth S. Effect of coconut shell biochar on the flexural properties of polylactic acid bio-composite filaments for fused deposition modeling. Sigma J Eng Nat Sci 2026;44(5):3304–3322.

INTRODUCTION

Demand for renewable materials and low-impact manufacturing keeps growing. Additive manufacturing suits that trend. FDM in particular gives designers freedom, keeps costs low, and can turn out customized parts with complex geometry and very little waste [1-3]. The process is simple: a thermoplastic filament melts in a heated nozzle and is laid down layer by layer. PLA, nylon, PETG, ABS, and TPU are the usual choices, mostly because they are easy to process and easy to buy [1, 4]. Fillers are one way to push these polymers further, and biochar is an attractive one. Coconut shell is cheap and plentiful, and the biochar made from it is porous, thermally stable, and rich in fixed carbon (75.25 wt% when we pyrolyzed it at 400 °C). Medical, automotive, and packaging uses are all plausible. The difficulty is in the details. Getting the biochar to disperse evenly, bond with the matrix, and still print cleanly is not straightforward. We looked at this problem for PLA-CBC filaments made from

*Corresponding author.
*E-mail address: vishalzdhimmar@gmail.com

This paper was recommended for publication in revised form by Editor-in-Chief Ahmet Selim Dalkilic

Published by Yıldız Technical University Press, İstanbul, Turkey
© Author. This is an open access article under the CC BY-NC license (http://creativecommons.org/licenses/by-nc/4.0/).

locally collected shell waste, and we tested how they behave in bending.

FDM parts generally have lower mechanical properties than conventionally manufactured parts [5, 6]. Weak interlayer adhesion, low tensile strength, and anisotropy limit the use of FDM parts in load-bearing applications [7]. Parameter optimization has also been applied to non-thermoplastic feedstocks. For a hydroxyapatite/collagen slurry, print speed and layer height were optimized by response surface methodology, which gave a dimensional error of 0.59%, within the 5% tolerance [8]. Musioł et al. [9] showed that biochar altered both the electrostatic properties and the degradation rate of PLA/P(3HB-co-4HB) blends, although their surface resistivity did not fall below the antistatic limit. The mechanical properties of FDM parts also depend greatly on process parameters such as raster orientation, layer height, nozzle and bed temperatures, infill pattern, and infill density [1, 10, 11]. PLA is more sensitive to these parameters than ABS [1, 10] was reported. The infill density and the layer height were optimized, and it was found that the flexural strength increases [11].

To improve the properties of unfilled thermoplastics, fillers and fibers have been added to the polymer matrix. In HAp/PLA filament feedstocks, all compositions showed pseudoplastic flow, and PLA/20HAp gave the best flow behavior for extrusion and printing [12]. Synthetic fibers enhance mechanical properties. Their disadvantage is that they come from non-renewable sources and have a heavy environmental footprint. That is why natural fibers have been drawing growing attention [13-23]. Adding 2% nanographene oxide to the resin and increasing the CFRP length from 20 to 50 cm increased the load capacity of strengthened beams by up to 64% [24]. Nanocrystalline cellulose (NCC) reduced post-printing cracks in a biomimetic HA/collagen composite and gave low shrinkage, 28% crystallinity, and thermal stability up to 650 °C [25]. Natural fibers such as flax, jute, and hemp are biodegradable and renewable and have a useful strength-to-weight ratio [14]. Bio-based and fiber-reinforced thermoplastics have also been developed for FDM [26, 27], and agricultural waste fillers have been reported to improve the thermal and mechanical behavior of PLA composites [18, 26, 27].

Biochar (BC) is a carbon-rich solid produced by pyrolysis of biomass. Due to its porous structure, high carbon content, and surface reactivity, it can be a potential filler for polymer composites [28-30]. The best filler content varies depending on the property considered. Tensile strength (16.4 MPa) and modulus (260.8 MPa) were greatest at 15% aluminum, whereas compressive strength (99.4 MPa) was greatest at 10% and strength decreased at higher aluminum content [31]. The addition of BC to PLA has been reported to increase its strength, impact resistance, and thermal stability [32]. Kane et al. [33] reported improved compostability and higher strength for PLA-BC composites. Huang et al. [34] reported an increase in tensile strength of 41.4% and impact strength of 32.1% with grapevine biochar. Musioł et al. [9] reported changes in the electrostatic properties and degradation rate of PLA/P(3HB-co-4HB) blends by biochar, but the surface resistivity remained above the antistatic limit.

However, biochar has been rarely studied as a filler in FDM filaments, and only a few studies report its effect on printed part properties. Anerao et al. [35] reported higher tensile strength, tensile modulus, and flexural modulus when biochar was added to PLA, while Pudełko et al. [36] and Zhang et al. [30] determined the filler contents that balance strength and brittleness in the composites. Aup-Ngoen and Noipitak [37] found that 25 wt% carbon-rich biochar from agricultural by-products increased the impact strength of PLA by 76% and the tensile modulus by 21%. Uniform dispersion, compatibility with the polymer matrix, and printability remain difficult to achieve.

Coconut shell is an abundant agricultural waste, and coconut shell biochar (CBC) is porous and had a fixed carbon content of 75.25 wt% when prepared at 400 °C in this study (Table 3). This study examines the effect of CBC content, infill pattern, and layer thickness on the flexural strength, modulus, and strain of PLA-CBC specimens printed by FDM.

MATERIALS AND METHODS

Materials

The PLA granules (3D850) supplied by Dream Polymer, Ahmedabad, are characterized by the mechanical and physical properties outlined in Table 1. Glycol was used as a plasticizer to enhance the flexibility and printability of the resulting filament. Coconut shells were sourced from local temples and markets. Chemical composition of coconut shell is given in Table 2.

The collected shells were first polished to remove fibres and dust from the shell and then processed using a milling machine to reduce them into small particles, as shown in Figure 1.

Table 1. PLA material properties as provided by dream polymer

Matrix	MeltvFlow index (g/10 min)	Density (g/cc)	Tensile modulus (MPa)	Tensile strength (MPa)	Elongation at yield (%)
PLA: 3D850	7-9	1.24	2315	51	3.31

Table 2. Chemical composition of coconut shell

Material	Lignin (Wt%)	Cellulose (Wt%)	Moisture (Wt%)	Hemicellulose and others (Wt%)	Ash (Wt%)
Coconut shell	29.35	24.2	7.073	38.56	0.68

Table 3. Fixed carbon analysis with different temperature

Material	Temperature ^{0}C	Moisture content (wt %)	Ash content (wt %)	Volatile matter (wt %)	Fixed Carbon (wt %)
CBC	350	5.25	26.02	1.54	67.19
CBC	400	4.1	12.5	8.15	75.25
CBC	450	3.5	14.48	25.67	56.35

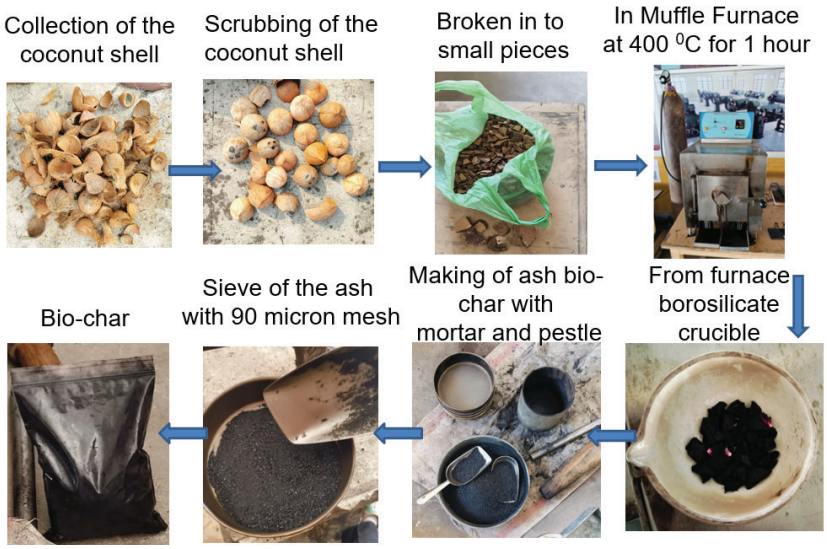


Figure 1. Preparation of BC from coconut shell.

The fixed carbon analysis of milled particles at varying temperatures was conducted. At 350 °C, the fixed carbon content was 67.19 wt%. Increasing the temperature to 400 °C resulted in a higher fixed carbon content of 75.25 wt%. However, when the temperature increased to 450 °C, the fixed carbon content decreased to 56.35 wt% as mentioned in Table 3. Therefore, 400°C provides the highest fixed carbon content (75.25%), making it the optimal temperature for enhancing the carbon content of CBC compared to the other temperatures tested.

After that, the char was ground into a fine powder with a particle size of approximately 90 microns. This powder was then placed back in the oven to ensure uniformity and readiness for subsequent filament production. After preparing all BC, it was also analysed at SICART, Vidyanagar for carbon and oxygen test and results are illustrated in Table 4.

Table 4. Carbon, hydrogen, nitrogen and oxygen analysis of CBC

Test Parameter	Name of the Instrument	Results
CHN (%)	CHN/O Analyser Elementer, Unicube	Carbon (%) - 77.84 Hydrogen (%) – 3.796 Nitrogen (%) - 0.17
Oxygen (%)	CHN/O Analyser Elementer, Unicube	Oxygen (%) – 15.113

Table 5. Temprature for extrusion process of filament manufacturing

Barrel zone	Feed zone [°C]	Compression zone [°C]	Mixing zone [°C]	Die zone [°C]	Screw speed [rpm]
PLA	195	195	220	210	30
PLA + CBC	180	185	195	195	20

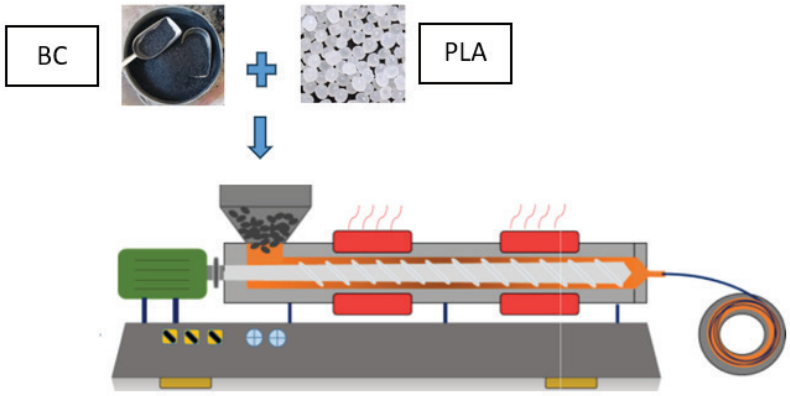


Figure 2. Illustration of manufacturing PLA-CBC composite filament for FDM process.

Development of Biocomposite Filament

Four distinct batches were prepared during the filament production process. In the first batch, PLA granules were mixed with 2% glycol using a batch mixer. The second batch was made up of PLA granules, 3% CBC, and 2% glycol. The third and fourth batches contained PLA granules with 2% glycol and 3% and 5% CBC, respectively. Glycol was added to the filament to enhance its printability and flexibility. Each batch was carefully mixed for consistency before being fed to a single-screw extruder. Table 5 indicates the temperature settings of each zone. Also, for pure PLA and PLA-CBC blends, a die pressure range of 2500–3000 PSI was applied. The batches were then heated, melted, and compounded in the extruder and then extruded in continuous filaments with a diameter of 1.75 mm. Figure 2 illustrates the production process for the PLA-CBC composite filament, while Figure 3 shows the four developed filaments.

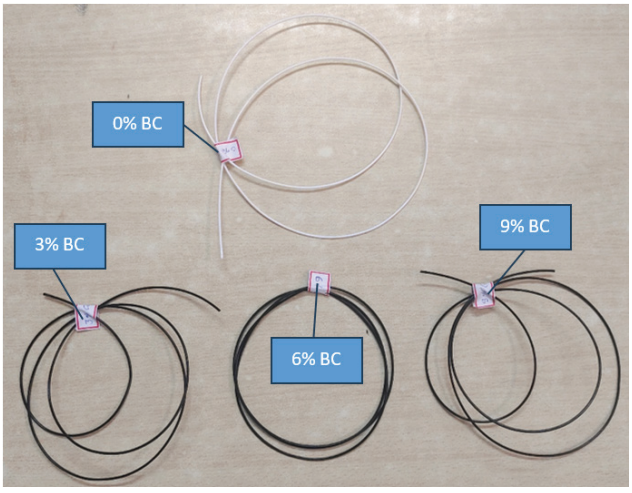


Figure 3. PLA-CBC composite filaments.

Process Parameters of FDM

According to existing literature, the process parameters employed in the FDM technique play a critical role in determining the mechanical properties of 3D-printed components [10, 35, 38-40]. Although certain parameters significantly affect mechanical performance, others like printing speed tend to exhibit a less pronounced influence on mechanical characteristics [29]. This study aims to specifically investigate the effect of four key process parameters layer thickness and raster angle (infill pattern) while keeping other process parameters at their constant values [2, 8, 10, 39]. A list of the constant, non-observed parameters is provided in Table 6.

Table 6. Process parameters of 3D printer at constant value

Process parameter	Value
Build orientation	Flat
Extruder temperature	215 °C
Bed temperature	60 °C
Nozzle diameter	0.4 mm
Printing speed	50 mm/s

Design of Experiments

Table 7 presents the three process parameters and their variation levels. A full factorial design was applied to obtain reliable results and identify the key factors influencing the response variable. Statistical analysis using Minitab software was performed to assess the effects of these parameters. Samples of the CBC-PLA composite were printed in the arrangements indicated in Table 8.

Table 7. Experimental design

Parameters	Units	Level 1	Level 2	Level 3	Level 4
Percentage of CBC (%)	-	3	6	9	0
Infill pattern	-	Parallel (0^0) 	Cross (-45^0, $+45^0$) 	Perpendicular (90^0) 	-
Layer Thickness	(mm)	0.15	0.20	0.25	-

Table 8. Full factorial design of experiment

Run Order	Percentage of CBC (%)	Raster Angle	Layer Thickness (mm)
1	9	Perpendicular (90^0)	0.2
2	6	Cross (-45^0, $+45^0$)	0.25
3	9	Cross (-45^0, $+45^0$)	0.25
4	9	Cross (-45^0, $+45^0$)	0.15
5	3	Parallel (0^0)	0.15
6	0	Perpendicular (90^0)	0.2
7	3	Perpendicular (90^0)	0.2
8	9	Perpendicular (90^0)	0.15
9	6	Perpendicular (90^0)	0.25
10	0	Cross (-45^0, $+45^0$)	0.15
11	6	Cross (-45^0, $+45^0$)	0.15
12	0	Parallel (0^0)	0.25
13	6	Perpendicular (90^0)	0.15
14	3	Perpendicular (90^0)	0.15
15	6	Parallel (0^0)	0.25
16	0	Perpendicular (90^0)	0.15
17	6	Cross (-45^0, $+45^0$)	0.2
18	0	Perpendicular (90^0)	0.25
19	9	Cross (-45^0, $+45^0$)	0.2
20	6	Parallel (0^0)	0.15
21	9	Perpendicular (90^0)	0.25
22	0	Parallel (0^0)	0.15
23	9	Parallel (0^0)	0.25
24	0	Parallel (0^0)	0.2
25	6	Perpendicular (90^0)	0.2
26	3	Cross (-45^0, $+45^0$)	0.25
27	9	Parallel (0^0)	0.15
28	3	Cross (-45^0, $+45^0$)	0.2
29	3	Parallel (0^0)	0.2
30	0	Cross (-45^0, $+45^0$)	0.25
31	9	Parallel (0^0)	0.2
32	3	Parallel (0^0)	0.25
33	6	Parallel (0^0)	0.2
34	3	Perpendicular (90^0)	0.25
35	3	Cross (-45^0, $+45^0$)	0.15
36	0	Cross (-45^0, $+45^0$)	0.2

Manufacturing and Testing of Bio-Composite Specimen

The G-code for exported CAD models for the flexure specimen as per ASTM D790 as shown in Figure 4, intended for 3D printing was produced using the Ultimaker Cura software. To create the CBC-PLA composite specimens as shown in Figure 5, a DAMBOY 3D printer by Engineering Techniques - FDM-based 3D printer was utilized. The parameters in Table 8 were defined, and for each experiment, the other variables were adjusted as outlined.

The flexue test is conducted in accordance with ASTM D790 using a TINIUS OLSEN/L-Series H50KL at CHARUSAT University, Anand, as shown in Figure 6, and the specifications of the machine are tabulated in Table 9. The flexural properties were assessed on five identical samples for each composition, and the average values were documented. The instrument software recorded and automatically computed the results. Figure 7 shows the 3D-printed specimens after flexure testing.

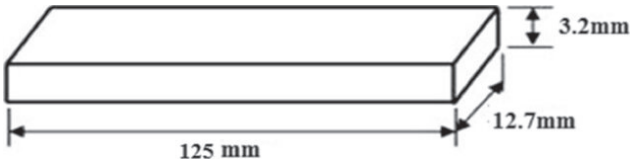


Figure 4. ASTM D790.

RESULTS AND DISCUSSION

Table 10 presents the flexural strength, modulus, and strain of PLA-CBC specimens printed with various CBC contents, infill patterns, and layer thicknesses. ANOVA showed that CBC content and infill pattern significantly affected all three responses, and layer thickness significantly affected strength and strain but not the modulus. The specimens with 9 wt% CBC generally had lower strength and modulus and higher strain than those with 3 and 6 wt% CBC, which suggests that high CBC loading reduces stiffness and increases deformation before failure. The parallel (0°) pattern gave the highest flexural strength, with a maximum of 124.8 MPa at 3 wt% CBC and 0.25 mm (run 32), and the perpendicular (90°) pattern gave the lowest. The



Figure 5. 3D printed flexure specimens.

Table 9. Specifications of UTM

Make/ Model	TINIUS OLSEN/ L – Series H50KL
Capacity	5000 kg
Construction	Solid Steel Crosshead with Sheet Panelling with Precision Ball
Force Measrment	50 KN, 50 N
Speed Control	0.001 to 500 mm/min
Dimensions	Height – 1620 mm Width – 720 mm Depth – 500 mm Depth – 500 mm Weight – 180 kg
Power	I/P supply voltage 230 V O/P supply voltage 48 V



Figure 6. Testing of flexure strength.

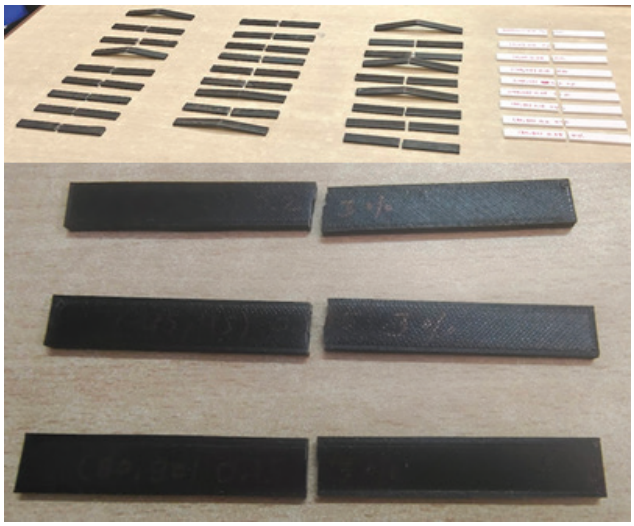


Figure 7. Printed flexure specimens after testing.

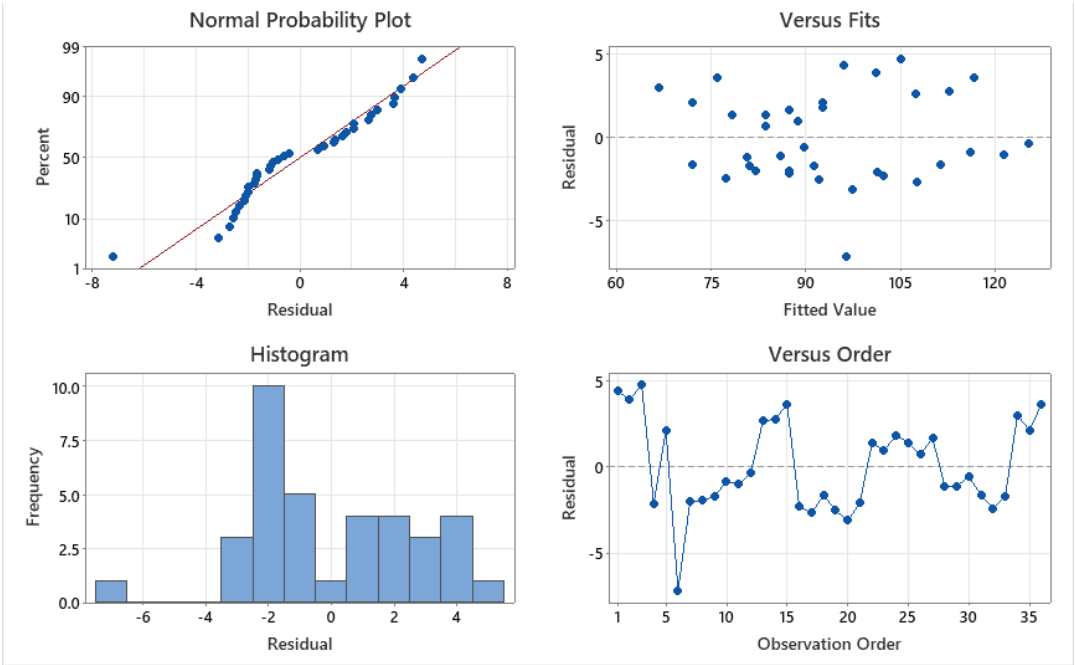


Figure 8. Residual graph of the flexure strength (MPa) with respect to biochar (%), infill pattern and layer thickness (mm).

cross (-45°, +45°) pattern gave the highest flexural strain. Strength and strain both increased with layer thickness from 0.15 to 0.25 mm. The reason for this trend was not examined and may relate to interlayer bonding or void content, which could be checked by microscopy of the fracture surfaces.

Analysis of Flexure Strength

ANOVA (Table 11) showed that CBC content, infill pattern, and layer thickness significantly affected the flexural strength of the printed specimens ($p<0.005$). CBC content accounted for 75.34% of the total variation, infill pattern for 15.02%, and layer thickness for 6.49%. The model explained 96.85% of the variation (adjusted R^2=96.06%, S=2.96 MPa), and its regression equation is given in Table 12. The residuals were approximately normally distributed (Fig. 8). According to the main effects (Fig. 9, Table 12), strength was highest at 3 wt% CBC and lowest at 9 wt%, higher for the parallel pattern than for the perpendicular pattern, and higher at 0.25 mm than at 0.15 mm.

Table 10. Average results of flexure test in terms of flexure strength, flexure strain and modulus

Run Order	Percentage of Biochar (%)	Infill Pattern	Layer Thickness (mm)	Flexural Strength (MPa)	Modulus (MPa)	Flexural Strain (%)
1	9	Perpendicular (90^o)	0.2	74.2 ± 9.5	2500 ± 236	4.2 ± 0.41
2	6	Cross (-45^o, +45^o)	0.25	94.5 ± 10.4	2200 ± 248	4.7 ± 0.34
3	9	Cross (-45^o, +45^o)	0.25	79.5 ± 9.4	2300 ± 198	4.8 ± 0.47
4	9	Cross (-45^o, +45^o)	0.15	70.4 ± 7.8	2100 ± 242	4.4 ± 0.44
5	3	Parallel (0^o)	0.15	115.2 ± 12.3	3500 ± 212	3.7 ± 0.41
6	0	Perpendicular (90^o)	0.2	85.4 ± 11.0	2800 ± 274	4.1 ± 0.38
7	3	Perpendicular (90^o)	0.2	104.8 ± 13.2	3400 ± 220	3.9 ± 0.32
8	9	Perpendicular (90^o)	0.15	69.8 ± 9.7	2400 ± 153	4 ± 0.54
9	6	Perpendicular (90^o)	0.25	89.1 ± 10.2	2300 ± 261	4.2 ± 0.36
10	0	Cross (-45^o, +45^o)	0.15	85.2 ± 12.7	3100 ± 242	4.2 ± 0.37
11	6	Cross (-45^o, +45^o)	0.15	84.9 ± 8.6	2400 ± 147	4.4 ± 0.47
12	0	Parallel (0^o)	0.25	109.8 ± 10.7	3300 ± 255	3.8 ± 0.52
13	6	Perpendicular (90^o)	0.15	79.7 ± 8.5	2500 ± 162	3.9 ± 0.46
14	3	Perpendicular (90^o)	0.15	99.9 ± 13.4	3300 ± 227	3.8 ± 0.38
15	6	Parallel (0^o)	0.25	99.2 ± 12.4	2700 ± 276	4.3 ± 0.53
16	0	Perpendicular (90^o)	0.15	80.1 ± 9.7	2900 ± 274	3.6 ± 0.38
17	6	Cross (-45^o, +45^o)	0.2	89.8 ± 12.3	2300 ± 183	4.6 ± 0.33
18	0	Perpendicular (90^o)	0.25	89.5 ± 11.1	2700 ± 185	3.9 ± 0.36
19	9	Cross (-45^o, +45^o)	0.2	74.9 ± 10.4	2200 ± 146	4.6 ± 0.41
20	6	Parallel (0^o)	0.15	89.6 ± 10.0	2500 ± 223	4 ± 0.42
21	9	Perpendicular (90^o)	0.25	79.6 ± 9.5	2600 ± 211	4.3 ± 0.45
22	0	Parallel (0^o)	0.15	100.3 ± 13.4	3500 ± 232	3.4 ± 0.47
23	9	Parallel (0^o)	0.25	89.2 ± 11.4	2400 ± 172	4.5 ± 0.34
24	0	Parallel (0^o)	0.2	105.1 ± 13.3	3400 ± 246	3.6 ± 0.39
25	6	Perpendicular (90^o)	0.2	84.3 ± 10.7	2400 ± 174	4 ± 0.42
26	3	Cross (-45^o, +45^o)	0.25	120.2 ± 14.6	3100 ± 189	4.5 ± 0.33
27	9	Parallel (0^o)	0.15	79.5 ± 9.8	2200 ± 167	4.1 ± 0.35
28	3	Cross (-45^o, +45^o)	0.2	115.5 ± 13.8	3200 ± 248	4.4 ± 0.32
29	3	Parallel (0^o)	0.2	120.3 ± 11.9	3400 ± 263	3.9 ± 0.41
30	0	Cross (-45^o, +45^o)	0.25	89.3 ± 9.9	2800 ± 191	4 ± 0.33
31	9	Parallel (0^o)	0.2	84.8 ± 9.7	2300 ± 167	4.3 ± 0.38
32	3	Parallel (0^o)	0.25	124.8 ± 13.1	3600 ± 254	4 ± 0.39
33	6	Parallel (0^o)	0.2	94.3 ± 9.7	2600 ± 211	4.2 ± 0.45
34	3	Perpendicular (90^o)	0.25	109.7 ± 13.0	3500 ± 239	4.1 ± 0.34
35	3	Cross (-45^o, +45^o)	0.15	110.1 ± 12.8	3300 ± 213	4.3 ± 0.37
36	0	Cross (-45^o, +45^o)	0.2	94.7 ± 9.8	3000 ± 191	4.4 ± 0.38

Table 11. ANOVA results for the flexure strength

Source of Variation	df	Sum of Squares (SS)	Contribution	Mean Square (MS)	F-Statistic (F)	P-value
Biochar Percentage	3	5870.7	75.34%	1956.90	223.00	<0.005
Infill Pattern	2	1170.6	15.02%	585.31	66.70	<0.005
Layer Thickness	2	505.5	6.49%	252.74	28.80	<0.005
Error (Residual)	28	245.7	3.15%	8.78		
Total	35	7792.5	100.00%			
Model Summary	S	R-sq	R-sq(adj)			
	2.96234	96.85%	96.06%			

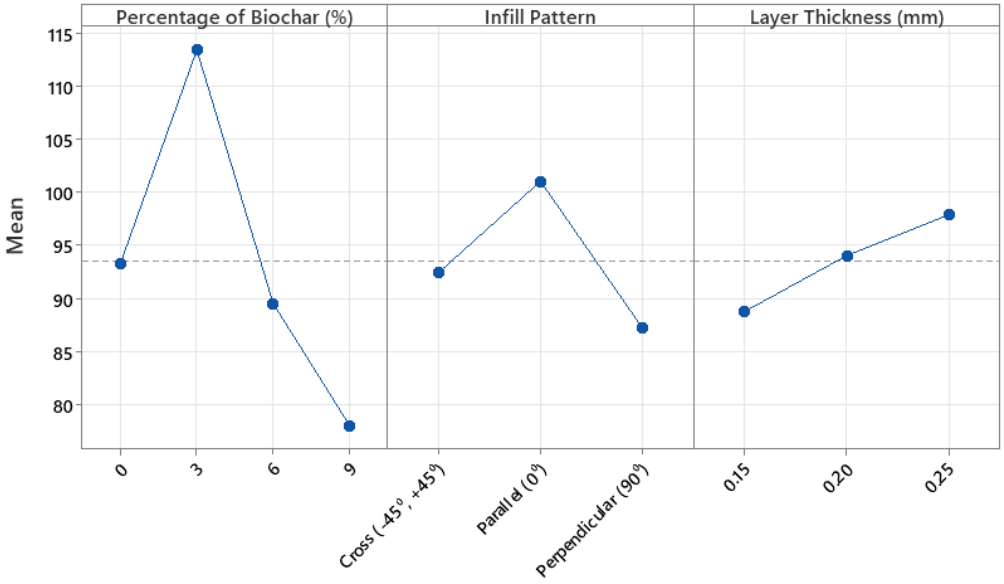


Figure 9. Main effect graph of the flexure strength with respect to biochar (%), infill pattern, and layer thickness (mm).

Table 12. Regression Equation for the flexure strength

Flexural Strength (MPa)=93.533 - 0.267 Percentage of Biochar (%)_0 + 19.856 Percentage of Biochar(%)_3 - 4.044 Percentage of Biochar (%)_6 - 15.544 Percentage of Biochar (%)_9 - 1.117 Infill Pattern Cross(-45^0,+45^0) + 7.475 Infill Pattern Parallel (0^0) - 6.358 Infill Pattern Perpendicular (90^0) - 4.808 Layer Thickness (mm)_0.15 + 0.475 Layer Thickness (mm)_0.20 + 4.333 Layer Thickness (mm)_0.25

Figure 10 shows the mean flexural strength at each combination of CBC content, infill pattern, and layer thickness, and Figure 11 gives contour plots of strength against CBC content and layer thickness for each infill pattern. The ANOVA model contained main effects only (Table 11), so interactions between the factors were not tested statistically. The main effects explained 96.85% of the variation in strength, which suggests that interactions contributed little. At 9 wt% CBC, the cross pattern gave lower strength (70.4 to 79.5 MPa) and higher strain (4.4 to 4.8%) than the parallel pattern (79.5 to 89.2 MPa and 4.1 to 4.5%). Strength and strain were both higher at 0.25 mm than at 0.15 mm. In contrast, Anerao et al. [35] reported that infill pattern had no significant effect on the flexural strength of PLA-biochar specimens, whereas infill pattern was significant here ($p<0.005$). The difference may be due to the factors and biochar source used in each study.

Analysis of Flexure Modulus

ANOVA (Table 13) showed that CBC content and infill pattern significantly affected the flexural modulus, whereas layer thickness did not. CBC content had the largest effect and accounted for 84.04% of the total variation ($F=80.63$, $p<0.005$), followed by infill pattern (6.20%, $F=8.93$, $p=0.001$). The effect of CBC was not monotonic. The modulus was highest at 3 wt% CBC (about 3367 MPa) and lower at 6 and 9 wt% (about 2433 and 2333 MPa) than for the unfilled filament (about 3056 MPa) (Table 14, Fig. 12). The parallel (0°) pattern gave the highest modulus (about 2950 MPa) and the cross pattern the lowest (about 2667 MPa). Layer thickness had no significant effect on the modulus over the 0.15 to 0.25 mm range (0.03% of the variation, $F=0.04$, $p=0.960$). The model explained 90.27% of the variation (adjusted $R^2=87.84\%$, $S=165.8$ MPa), and the regression equation is given in Table 14. The residuals followed an approximately straight line on the normal probability plot (Fig. 13), consistent with the normality assumption of ANOVA.

Figure 14 plots the mean modulus at each combination of CBC content, infill pattern, and layer thickness, and Figure 15 gives contour plots of the modulus against CBC content and layer thickness for each infill pattern. The ANOVA model contained main effects only (Table 13), so interactions were not tested statistically. The effect of layer thickness differed in direction with CBC content. In the unfilled filament, the mean modulus decreased from about 3167 MPa at 0.15 mm to about 2933 MPa at 0.25 mm, whereas at 9 wt% CBC it increased from about 2233 to about 2433 MPa, and at 3 and 6 wt% it varied by less than 70 MPa. These opposite trends may explain why

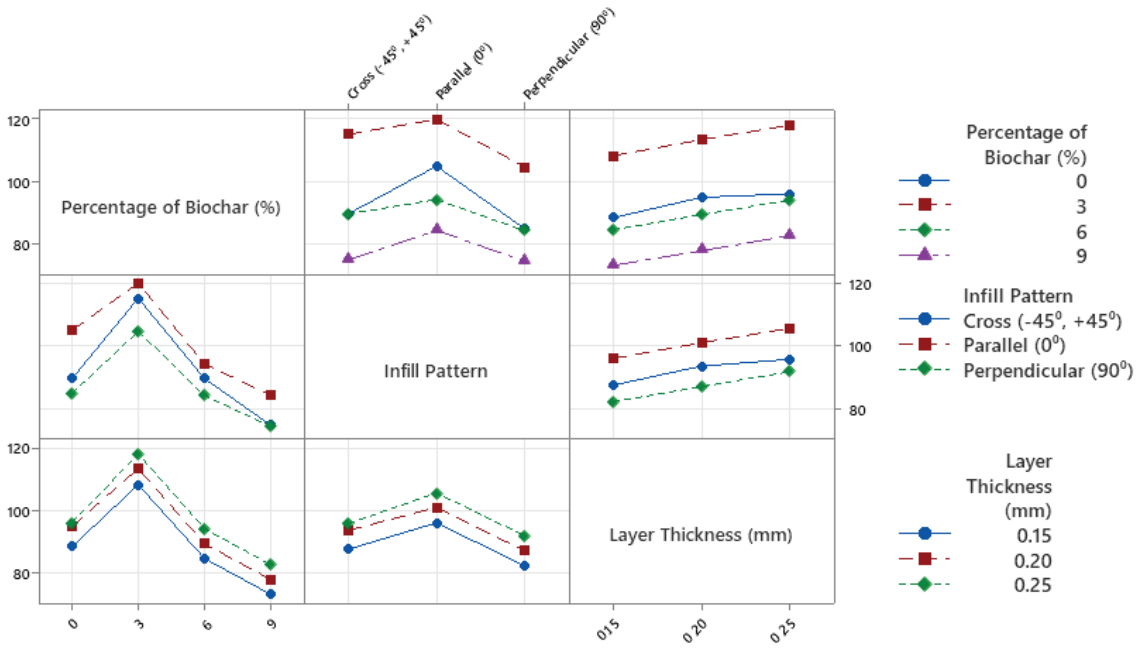


Figure 10. Interaction graph of the flexure strength (MPa) with respect to biochar (%), infill pattern and layer thickness (mm).

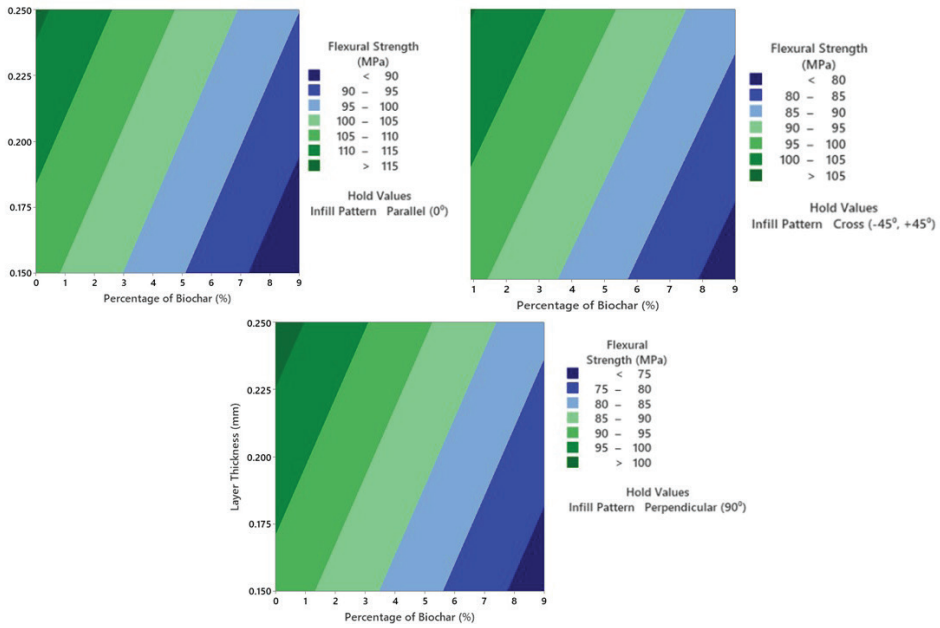


Figure 11. Contour graph of the flexure strength (MPa) versus biochar (%) versus layer thickness (mm) versus infill pattern.

Table 13. ANOVA analysis for the flexure modulus

Source of Variation	df	Sum of Squares (SS)	Contribution	Mean Square (MS)	F-Statistic (F)	P-value
Biochar Percentage	3	6647500	84.04%	2215833	80.63	<0.005
Infill Pattern	2	490556	6.20%	245278	8.93	0.001
Layer Thickness	2	2222	0.03%	1111	0.04	0.960
Error (Residual)	28	769444	9.73%	27480		
Total	35	7909722	100.00%			
Model Summary	S	R-sq	R-sq(adj)			
	165.771	90.27%	87.84%			

Table 14. Regression equation for the flexure modulus

Modulus (MPa)=2797.2 + 258.3 Percentage of Biochar (%)_0 + 569.4 Percentage of Biochar (%)_3 - 363.9 Percentage of Biochar (%)_6 - 463.9 Percentage of Biochar (%)_9 - 130.6 Infill Pattern Cross (-45°, +45°) + 152.8 Infill Pattern_Parallel (0°) - 22.2 Infill Pattern Perpendicular (90°) + 11.1 Layer Thickness (mm)_0.15 - 5.6 Layer Thickness (mm)_0.20 - 5 .6 Layer Thickness (mm)_0.25

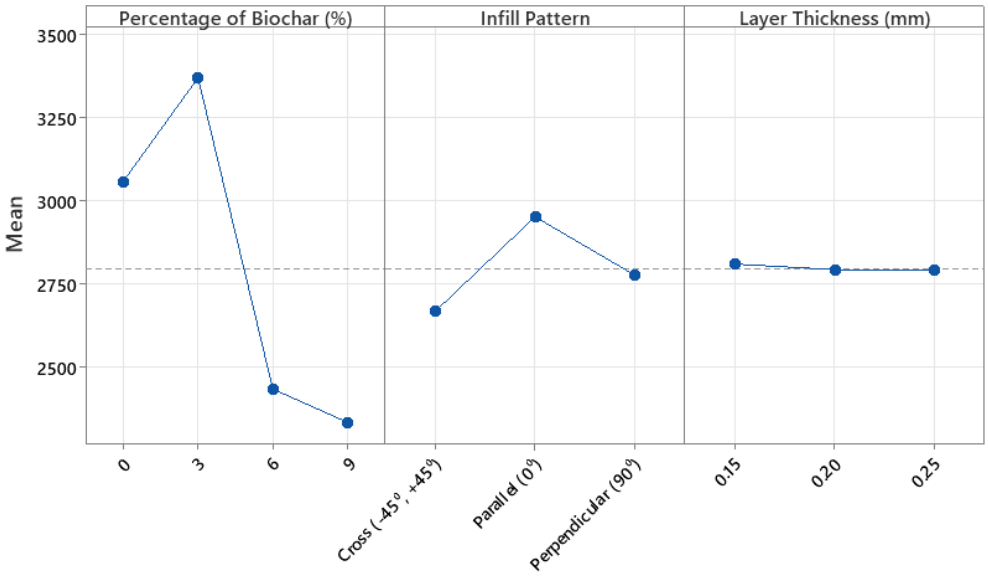


Figure 12. Main effect graph of the flexure modulus (MPa) with respect to biochar (%), infill pattern and layer thickness (mm).

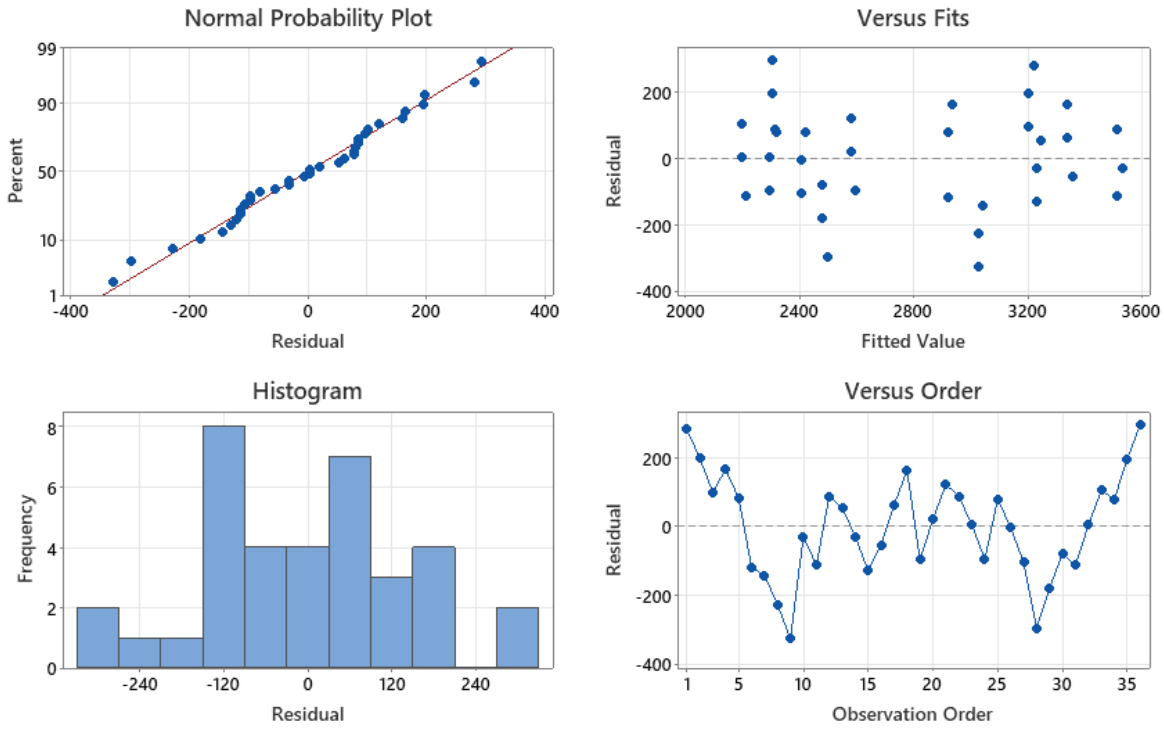


Figure 13. Residual graph of the flexure modulus (MPa) with respect to biochar (%), infill pattern, and layer thickness (mm).

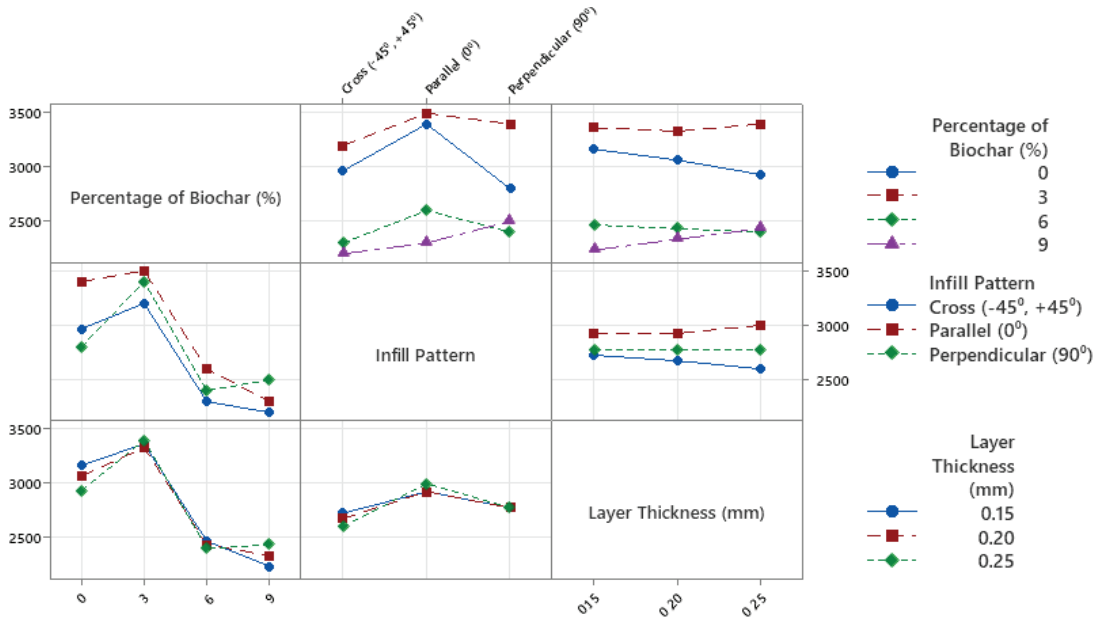


Figure 14. Interaction effect graph of the flexure modulus (MPa) with respect to biochar (%), infill pattern and layer thickness (mm).

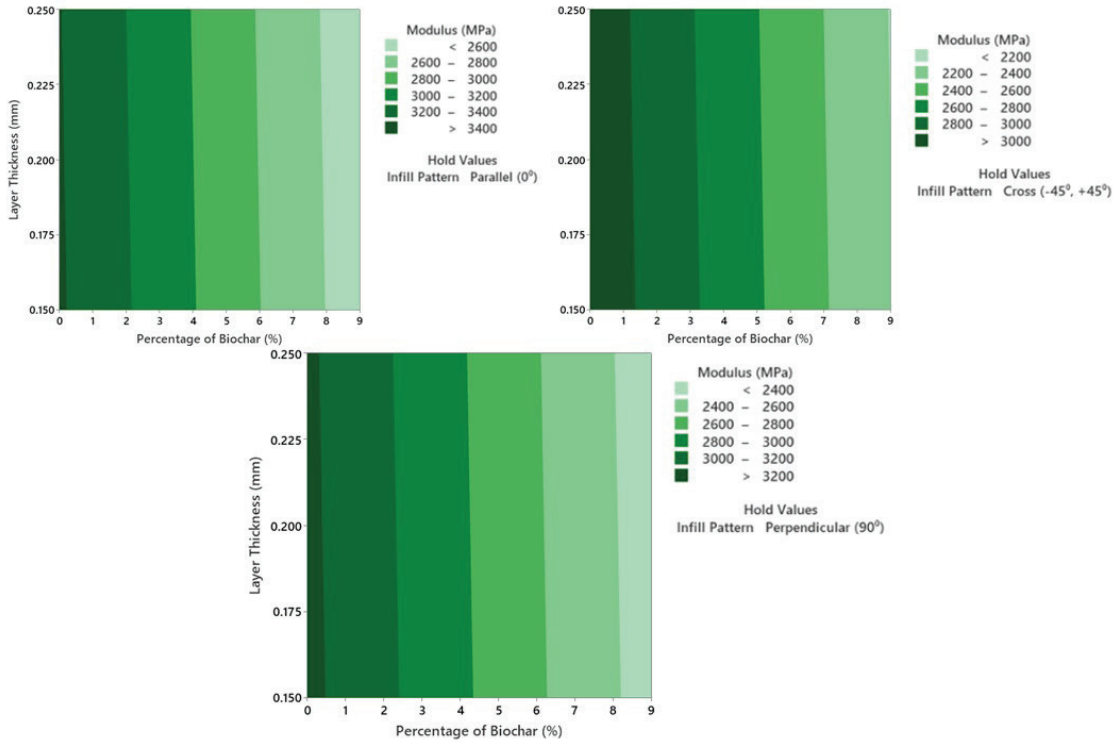


Figure 15. Contour graph of the flexure modulus (MPa) versus biochar (%) versus layer thickness (mm) versus infill pattern.

layer thickness had no significant main effect (p=0.960), and they suggest a possible CBC × layer thickness interaction that should be tested. The cross pattern gave the lowest mean modulus at 3, 6, and 9 wt% CBC, and the perpendicular pattern gave the highest at 9 wt% (about 2500 MPa). The maximum modulus at 3 wt% CBC is consistent with Anerao et al. [35], who reported the highest flexural modulus at 3 wt% rice husk biochar, although their best layer thickness (0.1 mm) was below the range tested here.

Analysis of Flexure Strain

ANOVA (Table 15) showed that CBC content, infill pattern, and layer thickness all had significant effects on flexural strain ($p<0.005$). Infill pattern had the largest effect and accounted for 43.74% of the variation ($F=50.83$), followed by CBC content (31.13%, $F=24.12$) and layer thickness (13.08%, $F=15.20$). Mean strain increased with CBC content, from about 3.89% at 0 wt% to about 4.36% at 9 wt% (Table 16, Fig. 16). The cross (-45°, +45°) pattern gave the highest strain (about 4.44%), compared with about 3.98% for the parallel and 4.00% for the perpendicular pattern. Strain also increased with layer thickness, from about 3.98% at 0.15 mm to about 4.26% at 0.25 mm. The model explained 87.95% of the variation (adjusted $R^2=84.94\%$, $S=0.126\%$), and the regression equation is given in Table 16. The residuals followed an approximately straight line on the normal probability plot (Fig. 17), consistent with the normality assumption of ANOVA.

Figure 18 plots the mean flexural strain at each combination of CBC content, infill pattern, and layer thickness, and Figure 19 presents contour plots of strain against CBC content and layer thickness for each infill pattern. The

Table 15. ANOVA analysis for the flexure strain

Source of Variation	df	Sum of Squares (SS)	Contribution	Mean Square (MS)	F-Statistic (F)	P-value
Biochar Percentage	3	1.1542	31.13%	0.38472	24.12	<0.005
Infill Pattern	2	1.6217	43.74%	0.81083	50.83	<0.005
Layer Thickness	2	0.4850	13.08%	0.24250	15.20	<0.005
Error (Residual)	28	0.4467	12.05%	0.01595		
Total	35	3.7075	100.00%			
Model Summary	S	R-sq	R-sq(adj)			
	0.126303	87.95%	84.94%			

Table 16. Regression equation for the flexure strain

Flexural Strain (%)=4.1417 - 0.2528 Percentage of Biochar (%)_0 - 0.0750 Percentage of Biochar (%)_3 + 0.1139 Percentage of Biochar (%)_6 + 0.2139 Percentage of Biochar (%)_9 + 0.3000 Infill Pattern Cros(-45^0, +45^0) – 0.1583 Infill Pattern Parallel(0^0) - 0.1417 Infill Pattern_Perpendicular(90^0) - 0.1583 Layer Thickness (mm)_0.15 + 0.0417 Layer Thickness (mm)_0.20 +0.1167 Layer Thickness (mm)_0.25

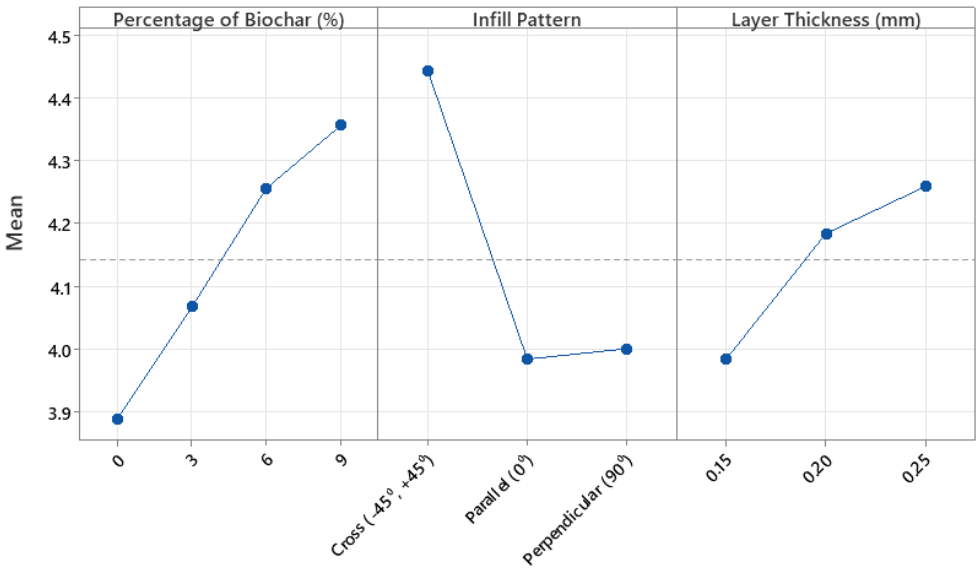


Figure 16. Main effect graph of the flexure strain with respect to biochar (%), infill pattern, and layer thickness (mm).

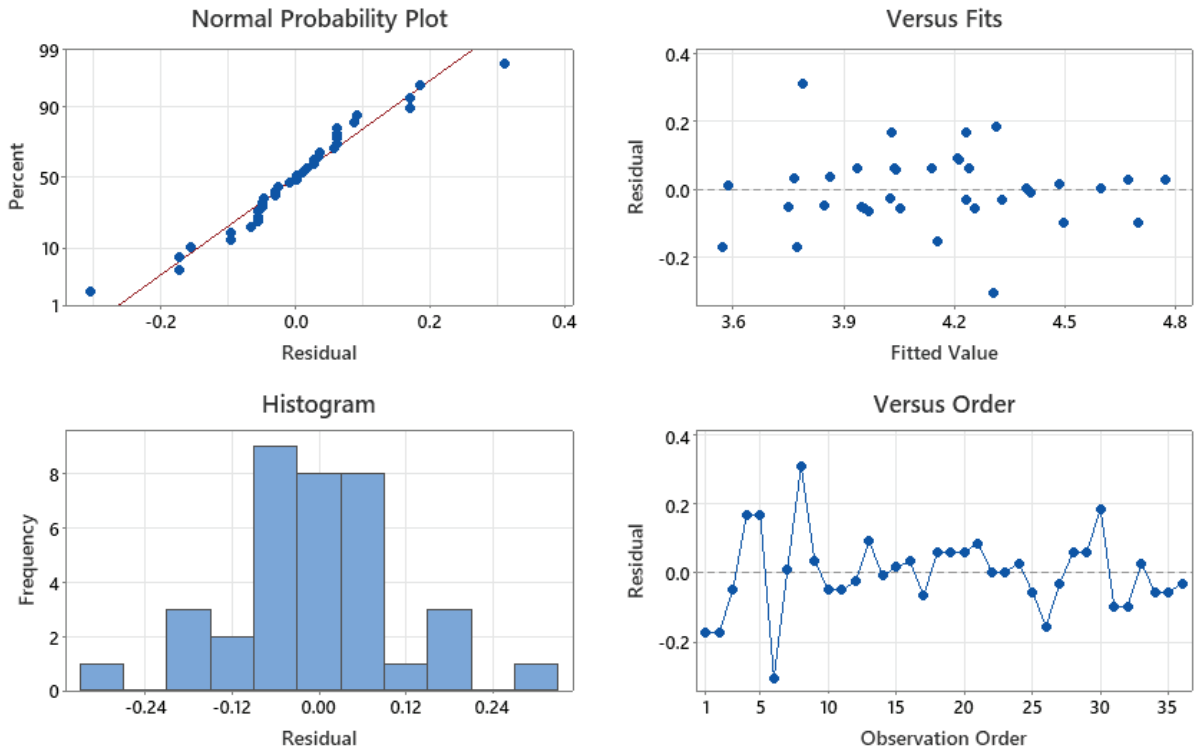


Figure 17. Residual graph of the flexure strain with respect to biochar (%), infill pattern and layer thickness (mm).

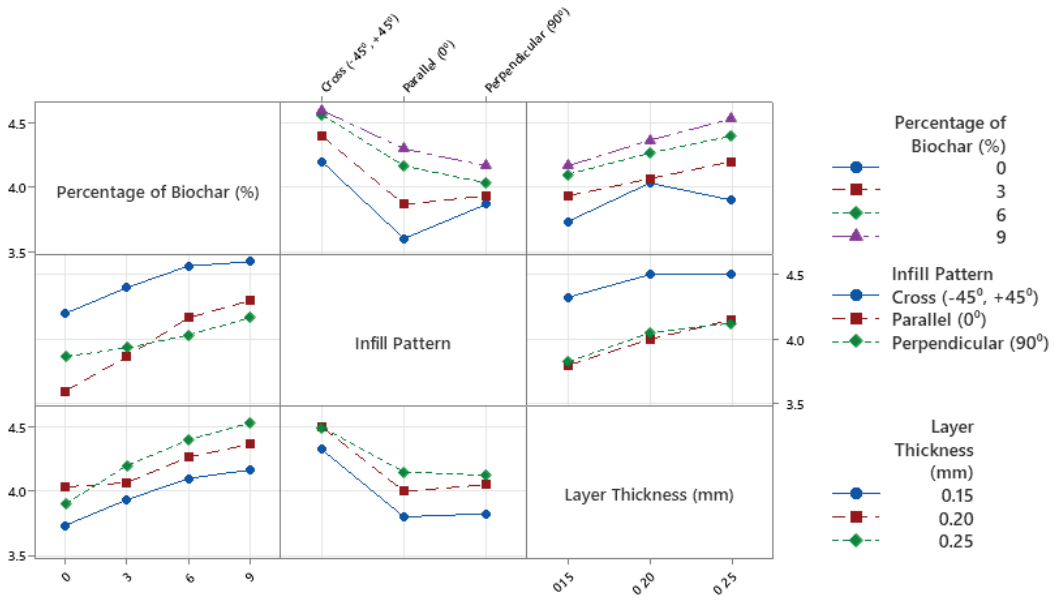


Figure 18. Interaction effect graph of the flexure strain with respect to biochar (%), infill pattern and layer thickness (mm).

ANOVA model contained main effects only (Table 15), so interactions were not tested statistically. At 3, 6, and 9 wt% CBC, the mean strain increased with layer thickness (for example, from 3.93% at 0.15 mm to 4.20% at 0.25 mm at 3 wt%), the same direction as the main effect. The cross (-45°, +45°) pattern gave the highest mean strain at every CBC content (4.20, 4.40, 4.57, and 4.60% at 0, 3, 6, and 9 wt%), about 0.4 to 0.5 percentage points above the other two patterns, and this difference did not increase with CBC content. These trends were not examined by microscopy, so

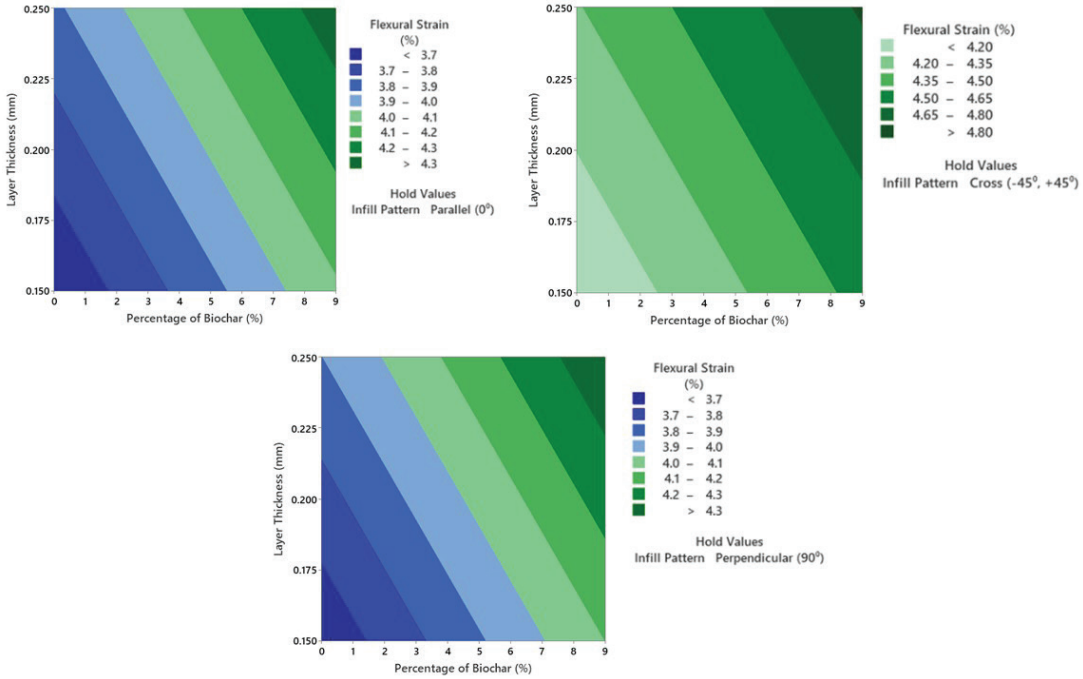


Figure 19. Contour graph of the flexure modulus versus biochar (%) versus layer thickness (mm) versus infill pattern.

mechanisms such as interlayer bonding or stress distribution remain untested. In contrast to Anerao et al. [35], who reported that flexural strain decreased above 3 wt% biochar in PLA, mean strain here increased with CBC content up to 9 wt%. The difference may be due to biochar source, particle size, or filament preparation.

Multi-Response Optimization

Multi-response optimization was carried out using the desirability function approach, which combines several responses into one composite desirability value and has been applied to machining [41] and slurry erosion [42]. The goals were to maximize flexural strength and flexural modulus and to minimize flexural strain, with the limits and targets given in Table 17 and weights and importance values of 1. [State why a lower strain was chosen as a goal.] The highest composite desirability (0.797) was obtained at 0 wt% CBC, a parallel (0°) infill, and a layer thickness of 0.15 mm (Table 18, Fig. 20). The predicted strength, modulus, and strain at this setting were 107.2 MPa, 3423 MPa, and 3.62%. The individual desirabilities were 0.68 for strength, 0.88 for modulus, and 0.85 for strain, so strength limited the composite value.

Table 17. Response optimization based on the desirability function

Response	Goal	Lower	Target	Upper	Weight	Importance
Flexural Strength (MPa)	Maximum	69.8	124.8	-	1	1
Flexural Strain (%)	Minimum	-	3.4	4.8	1	1
Modulus (MPa)	Maximum	2100.0	3600.0	-	1	1

Table 18. Solution of response optimization

Solution	Percentage of Biochar (%)	Layer Thickness (mm)	Infill Pattern	Flexural Strength (MPa) Fit	Flexural Strain (%) Fit	Modulus (MPa) Fit	Composite Desirability
1	0	0.150	Parallel (0°)	107.175	3.61583	3422.83	0.797327

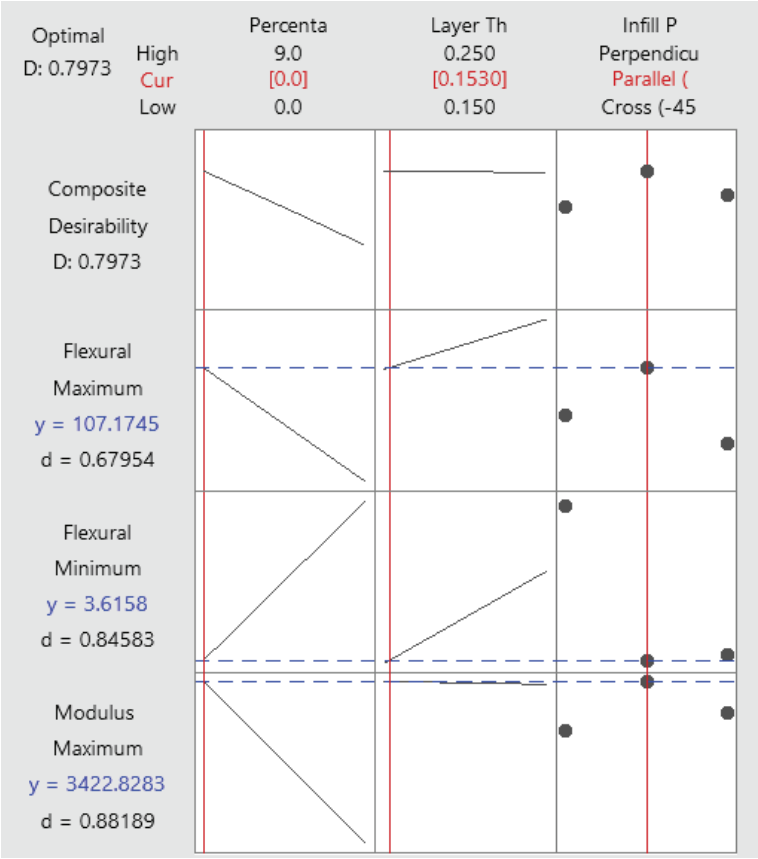


Figure 20. Optimization plot.

Validation

For the confirmation test, three samples were produced using the optimal parameters: 0% biochar, parallel (0°) infill pattern, and 0.15 mm layer thickness. Table 19 presents the results for flexural strength, strain, and modulus. As shown in Table 20, the mean absolute percentage error between the experimental and confirmation test values was 2.43% for tensile strength and 3.82% for modulus of elasticity.

Table 19. Confirmation result at optimum condition

Exp. No.	Percentage of Biochar (%)	Infill Pattern	Layer Thickness (mm)	Flexure Strength (MPa)	Modulus (MPa)	Flexure Strain
1	0	Parallel (0^0)	0.15	105.7	3490.4	3.71
2	0	Parallel (0^0)	0.15	108.25	3502.7	3.59
3	0	Parallel (0^0)	0.15	106.75	3420.6	3.6

Table 20. Mean absolute percentage error

Experimental result			Confirmation test result			Error %		
Flexure Strength (MPa)	Modulus (MPa)	Flexure Strain	Flexure Strength (MPa)	Modulus (MPa)	Flexure Strain	Flexure Strength (MPa)	Modulus (MPa)	Flexure Strain
107.175	3422.83	3.61583	105.7	3490.4	3.71	1.40%	1.97%	1.50%
107.175	3422.83	3.61583	108.25	3502.7	3.59	1.02%	2.33%	0.49%
107.175	3422.83	3.61583	106.75	3420.6	3.6	0.40%	0.06%	0.44%
				MAPE		1.62%	1.28%	0.30%

CONCLUSION

This study determined the effects of CBC content, infill pattern, and layer thickness on the flexural strength, modulus, and strain of FDM-printed PLA-CBC specimens using a full factorial design and ANOVA. CBC content had the largest effect on strength (75.34% of the variation) and modulus (84.04%). Both were highest at 3 wt% CBC and fell below the unfilled filament at 6 and 9 wt%, while strain increased with CBC content. The infill pattern had a significant effect on all three responses. The parallel (0°) pattern gave the highest strength and modulus, the perpendicular (90°) pattern the lowest strength, and the cross (-45°, +45°) pattern the highest strain. Layer thickness had no significant effect on the modulus (p=0.960), and strength and strain increased with layer thickness. Multi-response optimization, with strength and modulus maximized and strain minimized, selected 0 wt% CBC, a parallel (0°) infill, and a layer thickness of 0.15 mm (composite desirability=0.797). Three confirmation specimens at this setting agreed with the predictions, with mean absolute percentage errors of [0.93%, 1.46%, and 1.25%] for strength, modulus, and strain. The models contain only main effects and apply to the ranges tested. Microstructural analysis, dispersion, and degradation tests would be needed to explain the CBC trends, and biocompatibility or food-contact testing would be needed before any biomedical or packaging use.

ACKNOWLEDGEMENTS

Sincere gratitude is extended to Dr. Aksh Vyas, Post Dectoral Fellow, University of Alberta, Edmonton, Canada, Dr. Shakil Kagzi, Assistant Professor, SNPITRC, Bardoli, Gujarat, India, Dr. Yazad Jabbar, Associate Professor, SNPITRC, Bardoli, Gujarat, India and Dr. Rutal Mahajan, Assistant Profesor, Utica University, Utica, New York, USA for their invaluable guidance, insightful feedback and unwavering support throughout the research work.

AUTHORSHIP CONTRIBUTIONS

Vishal Dhimmar: Conceptualization, Methodology, 3D Printing, Testing, Analysis, Writing - Original Draft

Saurin Sheth: Supervision, Methodology, Writing - Review & Editing

DATA AVAILABILITY STATEMENT

The authors confirm that the data that supports the findings of this study are available within the article. Raw data that support the finding of this study are available from the corresponding author, upon reasonable request.

CONFLICT OF INTEREST

The authors reported that there are no competing interests to declare.

ETHICS

There are no ethical issues with the publication of this manuscript.

STATEMENT ON THE USE OF ARTIFICIAL INTELLIGENCE

Artificial intelligence was not used in the preparation of the article.

REFERENCES

[1] Kristiawan RB, Imaduddin F, Ariawan D, Ubaidillah, Arifin Z. A review on the fused deposition modeling (FDM) 3D printing: filament processing, materials, and printing parameters. Open Eng 2021;11:639–649. [CrossRef]

[2] Khalifah Mahameru RD, Faizin AK, Lamura MDP, Lestari WD. Optimization of 3D printing parameters for enhanced PLA tensile strength using the Taguchi method. Int J Automot Mech Eng 2025;22:12035–12047. [CrossRef]

[3] Zotti A, Paduano T, Napolitano F, Zuppolini S, Zarrelli M, Borriello A. Fused deposition modeling of polymer composites: development, properties and applications. Polymers (Basel) 2025;17:1054. [CrossRef]

[4] Kantaros A, Katsantoni M, Ganetsos T, Petrescu N. The evolution of thermoplastic raw materials in high-speed FFF/FDM 3D printing era: challenges and opportunities. Materials (Basel) 2025;18:1220. [CrossRef]

[5] Sotov A, Abdrakhmanova A, Zaytsev A, Zhuchenko E, Popovich A. Mechanical properties and flame resistance of 3D-printed coextruded continuous carbon fiber reinforced polycarbonate. Int J Eng 2025;38:1953–1967. [CrossRef]

[6] Hosseinzadeh MH, Azarniya A, Hassanpour M, Borhan Panah MR, Hajitabar A, Abbasi Bafetrat H, et al. Beyond standard ABS: recent advances in modified and composite filaments prepared for fused deposition modeling. Heliyon 2025:e43051. [CrossRef]

[7] Parandoush P, Lin D. A review on additive manufacturing of polymer-fiber composites. Compos Struct 2017;182:36–53. [CrossRef]

[8] Nurbaiti N, Tontowi AE, Widyastuti MG, Hoten HV, Ibrahim F, Muna N, et al. Process parameter optimization of 3D-printer machine using response surface method for printing hydroxyapatite/collagen composite slurry. Int J Eng 2023;36. [CrossRef]

[9] Musioł M, Rydz J, Janeczek H, Andrzejewski J, Cristea M, Musioł K, et al. (Bio)degradable biochar composites of PLA/P(3HB-co-4HB) commercial blend for sustainable future-study on degradation and electrostatic properties. Polymers (Basel) 2024;16:2331. [CrossRef]

[10] Rodríguez-Panes A, Claver J, Camacho AM. The influence of manufacturing parameters on the mechanical behavior of PLA and ABS pieces manufactured by FDM: a comparative analysis. Materials (Basel) 2018;11:1333. [CrossRef]
[11] Chokshi H, Shah DB, Patel KM, Joshi SJ. Experimental investigations of process parameters on mechanical properties for PLA during processing in FDM. Adv Mater Process Technol 2022;8. [CrossRef]
[12] Marzuki AP, Nasir MAM, Salleh FM, Ismail MH, Murat BIS, Ibrahim M. Initial study on rheological behavior of hydroxyapatites/polylactic acid composite for 3D printing filament. Int J Automot Mech Eng 2024;21:11064–11073. [CrossRef]
[13] Ali Z, Yan Y, Mei H, Cheng L, Zhang L. Effect of infill density, build direction and heat treatment on the tensile mechanical properties of 3D-printed carbon-fiber nylon composites. Compos Struct 2023;304:116370. [CrossRef]
[14] Ahmad MN, Ishak MR, Mohammad Taha M, Mustapha F, Leman Z. A review of natural fiber-based filaments for 3D printing: filament fabrication and characterization. Materials (Basel) 2023;16:4052. [CrossRef]
[15] Deb D, Jafferson JM. Natural fibers reinforced FDM 3D printing filaments. Mater Today Proc 2021. [CrossRef]
[16] Sapkota A, Ghimire SK, Adanur S. A review on fused deposition modeling (FDM)-based additive manufacturing (AM) methods, materials and applications for flexible fabric structures. J Ind Text 2024;54:15280837241282110. [CrossRef]
[17] Karthik K, Kolappan S, Ramesh V, Muthukumarasamy S. 3D printing with natural fiber composites: a review for advanced manufacturing applications. Interactions 2024;245:231. [CrossRef]
[18] Gigante V, Aliotta L, Canesi I, Sandroni M, Lazzeri A, Coltelli MB, et al. Improvement of interfacial adhesion and thermomechanical properties of PLA based composites with wheat/rice bran. Polymers (Basel) 2022;14:3389. [CrossRef]
[19] Prajapati AR, Dave HK, Raval HK. Effect of fiber volume fraction on the impact strength of fiber reinforced polymer composites made by FDM process. Mater Today Proc 2021. [CrossRef]
[20] Perroud T, Shanmugam V, Mensah RA, Jiang L, Xu Q, Neisiany RE, et al. Testing bioplastic containing functionalised biochar. Polym Test 2022;113:107657. [CrossRef]
[21] Khamvongsa M, Milton K, Faisal TR. Mechanical characterization of low-cost 3D FDM printed scaffolds fabricated with synthesized PLA/HA bio-composite filament. Ann 3D Print Med 2025;18:100194. [CrossRef]
[22] Vieira GM, Rosa MA, Wendhausen PAP, Martins MD. Ready-to-use composite fused deposition modeling filaments produced with polylactic acid and recycled Nd-Fe-B nanocrystalline powder for additive manufacturing of bonded magnets. IEEE Magn Lett 2025;16:1–5. [CrossRef]
[23] Sunay N, Kaya M, Kaynak Y. Chemical post-processing methods for enhancing surface properties of parts fabricated by additive manufacturing: a review. 2020.
[24] Halvaeyfar MR, Mirhosseini SM, Zeighami E, Joshaghani AH. Experimental study on bonding CFRP to fiber concrete beam considering the effect of using nanographene oxide in improving the mechanical properties of polyamine resin. Int J Eng 2022;35. [CrossRef]
[25] Herliansyah MK, Nurbaiti N, Tontowi AE, Widiastuti MG, Hoten HV. Effect of adding nanocrystalline cellulose on reducing micro-crack of three-dimensional printed hydroxyapatite/collagen composite. Int J Eng 2025;38:2537–2546. [CrossRef]
[26] Yan Y, Sun S, Pillay S, Ning H. Printability and mechanical behaviors of continuous polyamide fiber reinforced polycaprolactone composites. Polym Compos 2025;46:4491–4505. [CrossRef]
[27] Rahman MDA, Mahadi N, Choi HY, Shin EJ. Advancing sustainability in FDM 3D printing: development and characterization of bio-based TPU. J Polym Environ 2025. [CrossRef]
[28] Patel R, Dhimmar V, Kagzi S, Patel M. Investigation of fused deposition modelling process parameters in 3D printing for composite material (poly lactic acid and banana fibre). Int J Automot Mech Eng 2022;19. [CrossRef]
[29] Bhayana M, Singh J, Sharma A, Gupta M. A review on optimized FDM 3D printed wood/PLA bio composite material characteristics. Mater Today Proc 2023. [CrossRef]
[30] Zhang Q, Zhang D, Xu H, Lu W, Ren X, Cai H, et al. Biochar filled high-density polyethylene composites with excellent properties: towards maximizing the utilization of agricultural wastes. Ind Crops Prod 2020;146:112185. [CrossRef]
[31] Riyadi R, Ramadhana AVD, Dwiyatia ST, Sayefuddina EA, Kholila A, Paristiawanb PA. Mechanical characteristics and microstructure of natural fiber composite material with aluminum-reinforced for automatic clutch pads.
[32] Plamadiala I, Croitoru C, Pop MA, Roata IC. Enhancing polylactic acid (PLA) performance: a review of additives in fused deposition modelling (FDM) filaments. Polymers (Basel) 2025;17:191. [CrossRef]
[33] Kane S, Van Roijen E, Ryan C, Miller S. Reducing the environmental impacts of plastics while increasing strength: biochar fillers in biodegradable, recycled, and fossil-fuel derived plastics. Compos Part C Open Access 2022;100253. [CrossRef]

[34] Huang CC, Chang CW, Jahan K, Wu TM, Shih YF. Effects of the grapevine biochar on the properties of PLA composites. Materials (Basel) 2023;16:816. [CrossRef]

[35] Anerao P, Kulkarni A, Munde Y, Shinde A, Das O. Biochar reinforced PLA composite for fused deposition modelling (FDM): a parametric study on mechanical performance. Compos Part C Open Access 2023;12:100406. [CrossRef]

[36] Pudełko A, Postawa P, Stachowiak T, Malińska K, Dróżdż D. Waste derived biochar as an alternative filler in biocomposites - mechanical, thermal and morphological properties of biochar added biocomposites. J Clean Prod 2021;278:123850. [CrossRef]

[37] Aup-Ngoen K, Noipitak M. Effect of carbon-rich biochar on mechanical properties of PLA-biochar composites. Sustain Chem Pharm 2020;15:100204. [CrossRef]

[38] Sood AK, Ohdar RK, Mahapatra SS. Parametric appraisal of mechanical property of fused deposition modelling processed parts. Mater Des 2010;31. [CrossRef]

[39] Belarbi YE, Guessasma S, Belhabib S, Benmahiddine F, Hamami AEA. Effect of printing parameters on mechanical behaviour of PLA-flax printed structures by fused deposition modelling. Materials (Basel) 2021;14:5883. [CrossRef]

[40] Zandi MD, Jerez-Mesa R, Lluma-Fuentes J, Jorba-Peiro J, Travieso-Rodriguez JA. Study of the manufacturing process effects of fused filament fabrication and injection molding on tensile properties of composite PLA-wood parts. Int J Adv Manuf Technol 2020;108. [CrossRef]

[41] Maruda RW, Krolczyk GM, Feldshtein E, Nieslony P, Tyliszczak B, Pusavec F. Tool wear characterizations in finish turning of AISI 1045 carbon steel for MQCL conditions. Wear 2017;372–373. [CrossRef]

[42] Vyas A, Menghani JV, Patel PM, More SR, Paul CP, Patnaik A, et al. Characterization and optimization of slurry erosion behavior of SS 316 at room temperature. Trans Indian Inst Met 2021;74. [CrossRef]